PCCP

Accepted Manuscript

ROYAL SOCIETY OF CHEMISTRY

www.rsc.org/pccp

Journal Name

RSCPublishing

ARTICLE

Disorder Engineering of Undoped TiO_2 Nanotube Arrays for Highly Efficient Solar-driven Oxygen Evolution

Cite this: DOI: 10.1039/xoxxoooooox

Received ooth January 2012,
Accepted ooth January 2012

DOI: 10.1039/xoxxoooooox

www.rsc.org/

M. Salari,[a*] S. H. Aboutalebi,[b] A. Aghassi,[a] P. Wagner,[a] A. J. Mozer,[a] and G. G. Wallace[a *]

The trade-off between performance and complexity of the device manufacturing process should be balanced to enable the economic harvest of solar energy. Here, we demonstrate a conceptual, yet practical and well-regulated strategy to achieve efficient solar photocatalytic activity in TiO_2 through controlled phase transformation and disorder engineering in the surface layers of TiO_2 nanotubes. This approach enabled us to fine-tune the bandgap structure of undoped TiO_2 according to our needs while simultaneously obtaining robust separation of photo-excited charge carriers. Introduction of specific surface defects also assisted in utilization of the visible part of the sunlight to split water molecules for the production of oxygen. The strategy proposed here, can serve as a guideline to overcome the practical limitation in the realization of efficient, non-toxic, chemically stable photoelectrochemical systems with high catalytic activity in neutral pH under visible illumination condition. We also successfully incorporated TiO_2 nanotube arrays (TNTAs) with free-based porphyrin affording a pathway with an overall 140% enhanced efficiency, oxygen evolution rate of 436µl $h^{-1}$and faradic efficiencies over 100%.

Introduction

Photolysis, which is a general term to describe the photo-induced water splitting into H_2 and O_2 using sunlight, is a potentially clean and renewable proposition to address both energy and environmental challenges in a future green energy-driven economy. To this end, the ability of metal oxide semiconductors to reduce water to H_2 or oxidize it to O_2 will play an important role in the trend to move away from the reformation of fossil fuels as the world's primary hydrogen supply to the production of storable fuels using renewables (solar, hydro, etc) driven generated power. Therefore, the solar-driven electrolysis of water is an attractive alternative mainly due to the fact that the energy input required for water-splitting can be provided by clean solar energy. However, despite their great potential, the poor performance of these devices has prevented them from becoming a practical green and efficient technology. Moreover, most of semiconducting materials employed to date (e.g., CuO, (Al) GaAs and GaInP), although promising, suffer either from limited stability and degradation problems, high toxicity, and/or high final costs rendering them impractical for real-device applications. Therefore, the focus of current research is to realize photolysis from chemically stable non-toxic abundant materials in electrolytes near neutral pH conditions under practical 1-1.5 sun illumination [1, 2]. This goal, if realized, can enable architectural engineering of novel light-harvesting systems to yield solar fuel at practical cost targets.

As such, although the pristine bandgap of TiO_2 hinders the absorption of visible light, its low cost, abundance and high chemical stability has made it a hotspot for solar-related applications. Despite all its substantial characteristics, the large bandgap and fast electron- hole recombination are the main challenges to overcome in order to gain high efficiency for solar water splitting applications [3-7]. To this end, it has been proposed that an increase in Ti interstitials (Ti^{+3}) along with the introduction of oxygen defects can lead to the shift of the absorption peak from the UV region to the visible region [8]. Moreover, it has been also suggested that decreasing the concentration ratio of bulk defects to surface defects can lead to enhanced photocatalytic efficiency in the UV region [9, 10]. Additionally, to meet such a challenge, a combination of nanoscale size control, doping with other elements and bandgap engineering of TiO_2 have been proposed. Nevertheless, there is no systematic study to first establish which TiO2 polymorph is suitable for photoelectrochemical water splitting (PEC) and why, and second how surface disorder engineering can affect the overall performance of pure TiO_2 phase. Although there have been some attempts, answering these questions can help establish guidelines on the choice of starting material which can be further used in rational design of PEC devices [11, 12].

Herein, we systematically studied the bandgap structure of TiO_2 through controlled phase transformation of anatase to rutile by means of X-ray photoelectron spectroscopy (XPS) and photoluminescence measurements. Based on the obtained results, we propose an alternative strategy to improve the PEC performance of unadulterated TiO_2 by engineering the surface disorder of TiO_2 nanotubes and subsequently tuning the bandgap structure and increasing the surface donor density. The effective integration of favorable surface atomic structure with self-ordered nanotubular morphology of photoanode resulted in remarkable ability of the engineered structure as a PEC system. The strategy proposed here, can serve as a platform to overcome the limitations of PECs from a fundamental level leading the way to superior performance of TiO_2 based nanotube devices through further modifications such as chemical hydrogenation of TiO_2, treating the surface with active species, incorporation of noble-metal nanoparticles, etc. As a proof of concept, we employed different porphyrins as active photosensitizers to enhance light harvesting and consequently improve photochemical conversion efficiency.

Results and discussion

There have been persistent efforts to enhance the visible light absorption to create donor-acceptor states in various positions in the bandgap of TiO_2. For example, metallic (Fe and Nb) or non-metallic elements (such as N and C inclusions) could lead to structural modification of TiO_2 structure resulting in increased electrical conductivity and enhanced solar absorption characteristics of TiO_2 [3, 13, 14]. However, they adversely affect the UV region absorption due to the decrease in the incident photon to electron conversion in the UV region and an increase in the number of carrier recombination centres as well as decreased thermal stability [6]. On the contrary, self-doping of TiO_2, recognized as shallow donors, produces either oxygen vacancies or Ti interstitials (Ti^{+3}) [15-17]. Shallow donors are proved to extend the photocatalytic activity of TiO_2 from the UV to visible and infrared region with the additional benefit of trapping the charge carrier. Another important factor is the geometrical morphology of the TiO_2 photoanode. This is equally important for fast and directional charge carrier transfer and less undesirable recombination losses [6, 18]. It is known that TiO_2 architectures consisting of regular morphologies could perform more efficiently toward harvesting the light, due to better light scattering within an ordered architecture. Self-assembled TiO_2 nanotubes formed on a Ti foil by anodization method can therefore offer numerous advantages over non-ordered nano-particulate morphologies due to exhibiting unique physical traits such as better optical and electrical properties arising from quantum confinement effects [18-20]. Engineering the growth of more reactive energetic facets is another contributing geometrical factor which highly dominates the overall activity of TiO_2 surfaces and also accelerates the rate of reactions happening on the surface. It is equally important to adjust and manipulate the surface morphology of TiO_2 for efficiently photo-induced charge transportation and enhanced redox reaction taking place on the surface of the catalyst. Vertically aligned nanotubular geometry of TiO_2 is known very efficient for electrochemically-induced water splitting. As they provide high surface area with uniform, and directional ionic pass ways. Consequently they increase the light absorption depths and electron-hole separation due to increased solid liquid interface area and shortening the charge carrier transport distance to the electrolyte [6, 18].The photogenerated electrons and holes must travel from the bulk to the surface of the materials to react with adsorbed species. Thus, tubular structure with thinner wall thickness would result in more enhanced charge separation. Therefore, we prepared TiO_2 nanotubular architectures using a simple preparation method. These materials were utilized as the platform of choice to study the effect of controlled phase transformation of anatase to rutile on bandgap structure and facet reconstruction and consequently find suitable structures for water splitting (see supporting information for more details).

Glancing angle X-ray diffraction (GAXRD) measurements were performed to identify the phase distribution of the polymorphic TiO_2 along the nanotube arrays (Fig. 1a). Both anatase and rutile phases coexisted at samples annealed at temperatures below 500 ^{0}C with anatase being the dominant phase. However, increasing the annealing temperature resulted in an increase in rutile to anatase ratio. At 550 ^{0}C, anatase and rutile both existed equally, whereas, rutile was found to be the principle phase at samples annealed at higher temperatures; 600 ^{0}C and 650 ^{0}C. As we had demonstrated before [15-17] , heat treatment in an oxygen free atmosphere such as argon for prolonged period of time promoted anatase to rutile phase transformation. TNTAs are shown in the present work to have walls that expose high energy (111) and (200) surfaces in anatase and (210) in rutile (see supporting information for more details, Fig. S1). The formation of nanotubes in oxygen-free atmosphere therefore promotes the formation of high energy facets. The promotion of high energy facets in turn elevates the domination of electron traps associated with undercoordinated Ti atoms[21, 22] compared to hole traps (oxygen vacancies as predicted in our previous report [15]). Nevertheless, both electron and hole traps coexist in our system, while it is the electron trap that governs the whole process. To understand the effect of this phase transformation on the band structure and electronic states, we performed Photoluminescence (PL) and X-ray photoelectron spectroscopy (XPS) studies (see supporting information for more details, Fig. S2).

TNTA/600 ^{0}C showed a broad luminescence response ranging from 410 to 316 nm (3.024 to 3.92 eV) as well as the presence of two peaks at 438 (2.8 eV) and 467 nm (2.65 eV) indicating of the existence of self-trapped exciton luminescence activated by photons (Fig. 2(b)). The existence of these well-resolved PL peaks extending in the visible region can be contributed to the presence of oxygen vacancies or electron traps [23, 24]. According to the calculated electronic band structure of TiO_2 by Daude et al [25], the high energy PL bands correspond to the direct transitions; $X_1 \rightarrow X_1$ (3.45 eV), $X_2 \rightarrow X_1$ (3.59 eV), $\Gamma_5 \rightarrow \Gamma_4$ (4.05 eV), $\Gamma_3 \rightarrow \Gamma_5$ (4.81 eV), and lower energy PL band are assigned to the indirect transitions; $X_1 \rightarrow \Gamma_1$ (2.91 eV), $\Gamma_3 \rightarrow X_1$ (3.19 eV). The deconvoluted PL measurements of TNTA/600 ^{0}C, however, revealed the presence of shallow trap levels at 2.8 eV and 2.65 eV energy levels originating from undercoordinated Ti atoms and/or oxygen vacancies along the tubes [21]. The small shifts in peak positions observed here compared to the literatures [23, 24] are the result of different synthetic procedures, and degree of disorder and oxygen vacancies produced in our TNTAs during the heat treatment. The PL spectra obtained for the rest of the samples have been presented in supporting information.

Before measuring the photocatalytic activity of the TNTAs, we conceptually, studied the bandgap structure and dependency of the valance band of TNTA to the annealing temperature. Chemical bonding in transition metal oxides including TiO_2 is well described by molecular orbital theory. The valence and

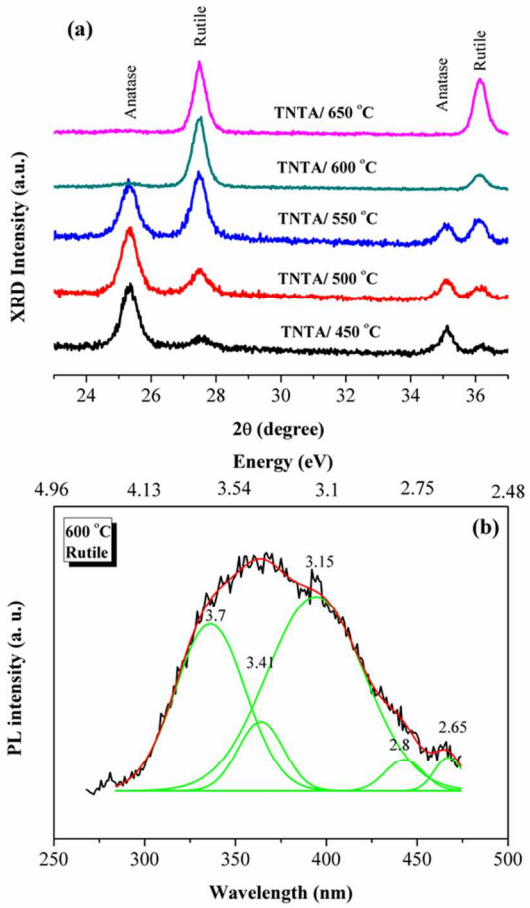

Figure 1 (a) GAXRD patterns for TNTA annealed at 450 - 650 ^{0}C under argon atmosphere. Small range of incident angle has been chosen to highlight the anatase and rutile phase change upon annealing temperature, and (b) PL spectra obtained for TNTA/ 600 ^{0}C, the black curve is the experimental results that deconvoluted into eight peaks (green curves), and the red curve is the summation of the deconvoluted peaks.

conduction band edge of both anatase and rutile are dominated by O 2p and Ti 3d orbitals, respectively [26, 27]. High resolution X-ray photoelectron spectroscopy (XPS) was, therefore, carried out to investigate the electronic valance band position of TNTAs annealed at different temperatures under argon atmosphere. The partially filled Ti 3*d* nonbonding states within the bandgap due to the existence of oxygen vacancies resulted in defect peaks near the valence band edge [26]. Out of four possible native TiO_2 disorders; Ti vacancy (V_{Ti}), O vacancy (V_O), and interstitial oxygen (I_O), interstitial titanium (I_{Ti}), T_{Ti} introduces a mid-gap state in TiO_2 nanocrystals about 0.5 eV below the conduction band minima [12, 19]. By introducing large amount of lattice disorder, mid-gap states are formed instead of discrete donor states. These can merge either with the valance or conduction band resulting in the so called band tailing which plays a crucial role in determining the electronic state [6] and electrochemical properties of TiO_2 [15-17]. This band-tailing potentially results in the modification of bandgap structure by introducing shallow donors with relatively low formation energy (see PL results). This consequently leads to improved visible light absorption. The band tailing (energy bending) could improve the light absorption of TiO_2 as it provides dominant centres for optical excitation and relaxation [12]. An additional advantage of the mid-gap states is that they act as trapping sites for photoexcited charge carriers and prevent the rapid charge recombination resulting in an overall improvement on PEC reactions. The bending of energy bands due to the formation of mid-gap electronic states introduces a net negative charge on the surface of TiO_2 as free electrons from the bulk are trapped into surface states at the semiconductor/electrolyte surface [15, 28]. In fact, if enough larger amount of lattice disorders are introduced into the system, lower energy mid-gap states are formed which can potentially merge valence band and conduction band edges.

The valence band maximum (VBM) was determined by extrapolating the linear portion of the low energy edge of the valence band to the spectral baseline (see supporting information for more details). The assignment of the observed PL peak at visible region to electron traps associated with undercoordinated Ti^{3+} (when occupied) also suggests the existence of located surface traps at energies about 0.5–1.0 eV below the conduction band [21, 29]. Fig. 2 shows the VBM of all samples as determined by XPS measurements. The VBM edge for the as-prepared TNTA (amorphous TiO_2) was calculated to be 3.906 eV and the conduction band minimum is positioned at 0.66 eV (see supporting information for more details, schematic illustration as an inset in Fig. 2(a)). The maximum valence edge of TNTA/450 ^{0}C and TNTA/500 ^{0}C (dominant anatase phase) found out to be at 3.823 eV. However, upon annealing at 500 ^{0}C the VBM edge blue shifted toward the vacuum level at 2.77 eV due to a band tailing driven from surface reconstruction. Increasing annealing temperature led to an observed shift of the band tailing towards more negative energies. As an example, the edge of VBM (band tail) for TNTA/650 blue shifted to 1.751 eV due to more oxygen depletion from the surface or induced titanium interstitials [15]. According to the XRD measurements anatase is the governing phase at low temperatures. Therefore, photoexcited electrons can transfer from O 2*p* orbitals to Ti 3*d* of anatase. Whereas, in TNTAs annealed at higher temperature with rutile as the dominant phase, the optical charge transition can happen between O 2*p* and Ti 3*d* orbitals of rutile. The charge transfer can also occur between the lower-energy mid-gap states and conduction band similar to the photoexcitation from the VB to the CB of TiO_2. This, in turn can lead to the introduction of localized photoexcited electrons and holes and consequently the injection of photoexcited electrons to adsorbed species. This prevents electron hole recombination and enhances the charge separation life time.

Thermodynamically, water splitting is a non-spontaneous process requiring a bandgap energy barrier of 1.23 eV and any additional overpotential needed to drive catalysis. Generally, this overpotential at least adds an additional 0.6 eV to the bandgap barrier. It should also be noted that a good photovoltaic semiconductor can merely generate around 70% of its bandgap in photovoltage at 1 sun. Thus, the minimum bandgap required to drive photolysis is greater than 2 eV [1, 14]. In a practical setup, once *e-h* separation is realized, electrons will be injected to chemisorbed water molecules on the cathode surface to generate H_2. On the other hand, holes will be scavenged by H_2O on the anode surface, which is oxidising H_2O to O_2 [7]. According to the water Pourbaix diagram, shown in Fig. S2, hydrogen evolution reaction (HER) and oxygen evolution reaction (OER), under near-neutral pH conditions, happen at a potential around -0.4 eV and 0.8 eV, respectively. Upon irradiation of TNTA, providing energy absorption equal or greater than the TNTA bandgap of TNTA, electrons excite

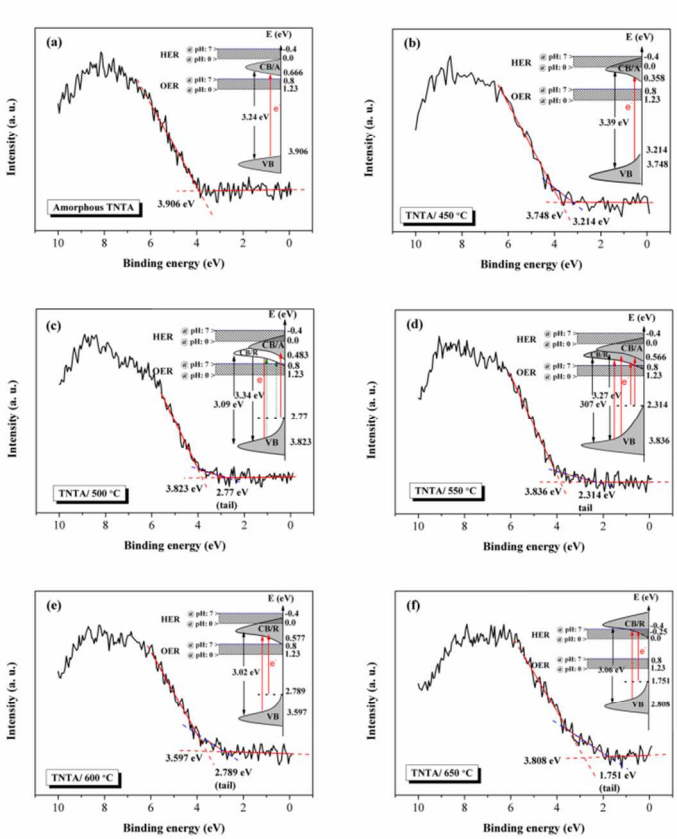

Figure 2 (a) XPS valence band spectra obtained along with schematic illustration of DOS, as an inset for amorphous TNTA and TNTA annealed at different temperatures. The red line highlights the linear extrapolation of the experimental curves; VB is donated as the valence band, CB/A as anatase conduction band, CB/R as rutile conduction band, HER as hydrogen evolution reaction, and OER oxygen evolution reaction. The principal charge transfer has shown with red line, while the minor charge transfer coded by dash green line. Fundamentally, anatase and rutile has indirect and direct bandgap, respectively [30].

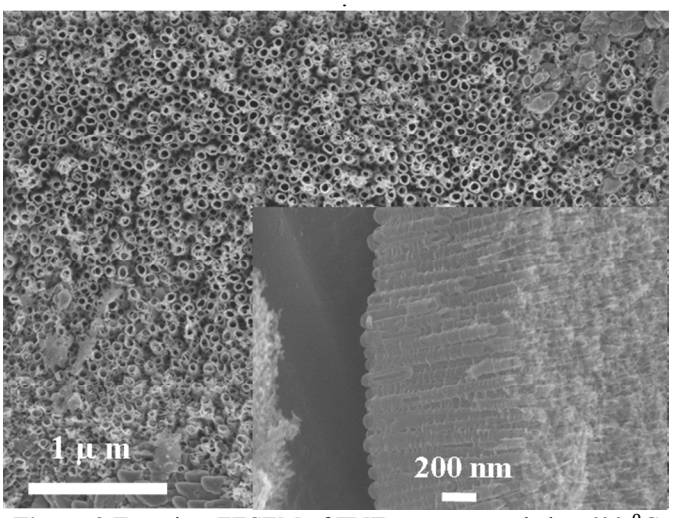

Figure 3 Top view FESEM of TNT arrays annealed at 600 ^{0}C for 5 h under argon atmosphere and typical side view FESEM of as prepared TNTA as an inset leading to formation of disordered layers surrounding crystalline core around a few nanometres in thickness.

from valence band to the conduction band leading to an electron-hole separation. Comparing the DOS diagrams depicted as insets in Fig. 2, one can conclude that, upon illumination, both amorphous TNTA and TNTA/450 ^{0}C require higher energy photons to excite the electron from valence band to the conduction band, due to their large bandgaps. However, the band tailing created at TNTA/500 ^{0}C can potentially subsidize the required energy for photoexcitation phenomenon. TNTA/550 ^{0}C can provide electrons with enough energy to overcome the water splitting potential plus the necessary overpotential. TNTA/550 ^{0}C, both anatase and rutile phase coexist equally in the system which in turn leads to bandgap narrowing. The electron can then potentially travel from the band tail states as well as valence band to the conduction band of anatase and rutile. Narrowed bandgap structure along with the shallow trap states favourably enhances the PEC performance. According to the half-cell reaction of water oxidation, ($2H_2O \rightarrow O_2 + 4H^+ + 4e$) the accumulation of H^+ in vicinity of the anode electrode results in localized pH degradation and shift the required potential from 0.8 towards 1.23 eV (Fig. S4, Pourbaix diagram). Therefore, the energy resulted from the electron transportation from band tail states to the conduction band would be around 1.5 eV which does not satisfy the required energy for water disassociation. In contrast, the tailored bandgap structure obtained for the sample annealed at 600 ^{0}C provides enough energy (1.95 eV) in the pH ranging from neutral to acidic conditions. Further annealing at 650 ^{0}C would yield much narrower bandgap energy of 3.06 eV along with maximum valence band edge of 1.751 eV. Even though, the UV and visible region absorption would have enough energy to generate O_2, the structural collapse and peeling off from the substrate would remain as a challenge for the use of this electrode for photocatalysis or electrochemical applications [15].

Fig. 3 shows a typical top view FESEM image of anodic TiO_2 nanotube arrays (TNTA) annealed at 600 ^{0}C. The inner pore diameter and the tube length of tubes are calculated to be around 36±5, and 750 nm, respectively. The wall thickness of TNTA is also observed to be around 10 nm. The thinner tube thickness benefits the charge injection in TNTA hence higher PEC efficiency. Despite bulk defects unfavourably promoting *e-h* recombination and decreasing photocatalytic efficiency, as explained earlier, the surface defects such as oxygen vacancies can serve as charge carrier traps and adsorption sites; where the charge will be injected to the adsorbed species, and significantly increase the carrier life time and promote the photocatalytic efficiency [9]. Accordingly, it is safe to assume that in our case study, the most structural defects have been introduced to the outer layers of TNTA due to the formation of very thin tubes (wall thickness of 10 nm). Consequently, disorders would participate favourably in photocatalytic reactions.

Since TiO_2 is an n-type semiconductor and participates in the water oxidation under forward biased potentials, the oxygen generation in the water splitting is of our primary interest to measure the photoelectrochemical activity of our engineered architectures. Two different types of porphyrins, free-based porphyrin and Cu doped porphyrin (Cu-porphyrin) were incorporated on TNTAs to enhance the photoexcited electrons at the anode and reduce overpotential associated with water oxidation. The highly reduced TNTAs and hybrid TNTAs were used as the photoanode and the photocurrent responses were

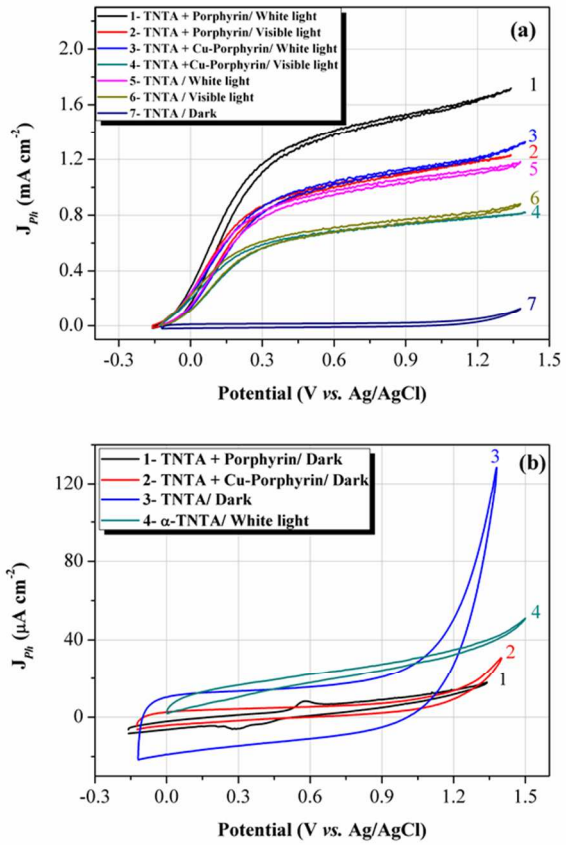

Figure 4 (a) Variation of photocurrent density *vs.* measured potential as a function of TiO_2 crystal under Xe lamp irradiation of 150 mW cm^{-2}, and (b) overlaid photocurrent generated by crystallized TNTA, porphyrin containing electrodes in dark condition compared with α- TNTA (amorphous TNTA) under Xe lamp irradiation of 1000 mW cm^{-2}.

studied as a function of biased potential in dark, and white light illumination, shown in Fig. 4 (a).

The obtained photocurrent of TNTA at 0.63 $V_{Ag/AgCl}$ (1.23 V_{RHE}, at pH of 7) was 0.98 mA cm^{-2} which is higher than the photocurrent achieved by chemically reduced TiO_2 nanotubes at the same potential (0.732 mA cm^{-2} at 1.23 V_{RHE} [6]). The yielded photocurrent for the TNTA- porphyrin showed the highest value over the entire potential window whereas, the current obtained for TNTA/Cu-porphyrin was comparable with the pure TNTA in coloured range and showed slightly improved photocurrent under white light irradiation. Achieving low photocurrent onset potential as well as low saturated potential are particularly important factors in order to maximize the PEC efficiency of a device, as it reduces required applied potentials [13]. All samples showed onset potentials at very low biased potentials suggesting an efficient charge carrier separation. For instance, in the TNTA/porphyrin, the photo generated current drastically increased at an onset potential of -0.14 V *vs.* Ag/AgCl reaching a saturated current of 1.16 mA cm^{-2} at 0.3 V then gradually increased by the applied potential reaching 1.72 mA cm^{-2}, indicating photogenerated *e-h* separation resulting from the electric field [6].

All samples including pure TNTA showed enhanced current densities under the coloured range light illumination. As mentioned earlier, the coexistence of both uncoordinated Ti atoms and oxygen vacancies significantly contribute to the enhancement in visible light adsorption and hence increase in current density. Owing to valance band edge of 2.78 eV in TNTA/600 ^{0}C (Fig. 2 (c)), the photoexcited electrons transferred from oxygen vacancies levels to the CB and mid-gap states are involved in the water oxidation. This is because their energy levels are well beyond the oxygen evolution reaction potential. Therefore, the high photocurrent observed for the pure TNTA in the coloured ranged illumination can be attributed to these electron transportations (Fig. 4 (a) Line-6).

Fig. 4 (b) also compares typical current densities obtained from the annealed TNTA with and without porphyrins in dark condition as well as the photocurrent generated by the amorphous TNTA under illumination. TNTA showed an enhanced area under the CV curve at the scan rate of 50 mV s^{-1}, which is indicative of good charge propagation and supercapacitive properties of TiO_2. The tubular structures can provide directional pathways for electron transfer [15, 31]. Gaining decreased current densities for the porphyrin-containing electrodes, we concluded that porphyrins efficiently covered the tubular channels resulting in a partial blockage of the layers leading to reduced ionic movement and propagation inside the tubular architecture. The surface morphologies were also examined using an optical microscopy, shown in Fig. S5 (Supporting Information). The surface colour changes confirmed incorporation of TNTA with the dye molecules which was fairly uniform on the entire surface. In comparison with its crystalline counterpart, the amorphous TNTA contributed negligible photocurrent density even under very intense light irradiation (1000 mW cm^{-2}). This is due to irregular crystalline phases which act as preferential recombination sites for the excited electrons. In contrast, annealing process increases the crystallinity and consequently enhances charge transfer and photocatalytic activity [32].

Porphyrin and porphyrin derivatives polymers are well recognized for their remarkable light harvesting abilities in the visible range of light spectra. This is attributed to existence of different functional anchoring groups such as hydroxyl carboxylate and sulfonate groups [33]. In the present work, we used the phosphonate anchor porphyrins. The molecular structure of the dye sensitizers are given in Supplementary information (Fig. S6). The hybrid structure comprising of TNTA and free-based porphyrin showed an enhanced current density resulting from the enhanced electron injection of porphyrin into the conduction band of TiO_2. More work is currently underway in our research group in order to determine the best porphyrin and optimise the dye-uptake procedure in order to increase the PEC efficiency.

In order to examine the light response of TNTA, linear sweep voltammetry (LSV) test was performed at voltage scan rate of 5 mV s^{-1} while the light was chopped off at regular intervals (Fig. 5(a)). The generated current for both TNTA with and without porphyrin is corresponded to the light illumination as there is sharp down-shift to negligible current values, whenever the light is switched off.

Fig. 5(b) shows solar light energy to chemical energy conversion efficiency (η) *vs.* potential calculated using the following equation (Eq. 1)[34, 35]:

$$\eta = J_{ph}[1.23-(V_{app}-V_{ocp})]/I_0 \quad \text{Eq.1}$$

where, J_{ph} (mA cm^{-2}) is the photocurrent density at the measured potential, I_0 (150 mW cm^{-2}) is the light intensity, V_{app} (V) is the applied bias, V_{ocp} (V) is the open circuit potential, and 1.23 corresponds to the required potential for water splitting. Photocurrent efficiency for TNTA is calculated to be

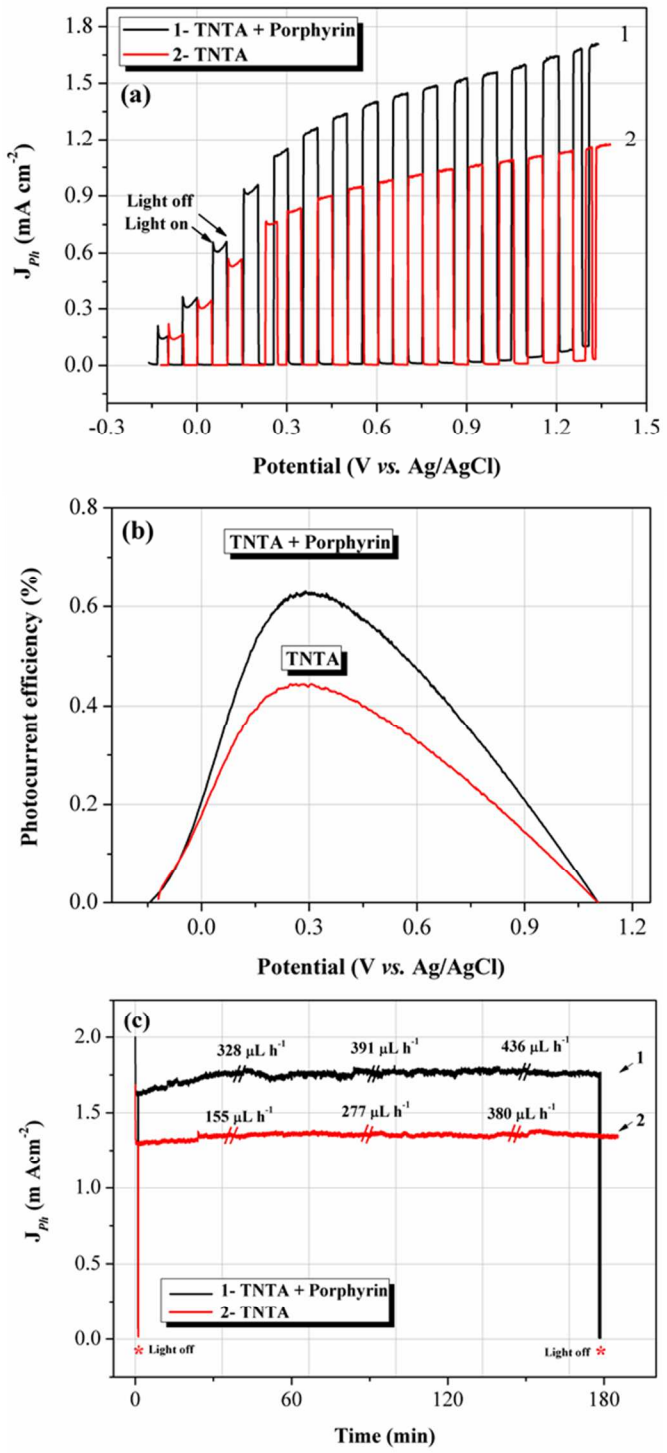

Figure 5 (a) linear sweeps voltammetry (LSV) with scan rate of 5 mVs^{-1} under chopped off simulated light powered at 150 mW cm^{-2}, (b) calculated photoconversion efficiencies as a function of applied potential, and (c) amperometric measurements (*i-v* curve) collected from TNTA with and without porphyrin (at 1.1 V).

0.45 %, which is almost two times higher than the value reported for nanorod *n*-GaN (0.26% at 0.8 V) [36]. The porphyrin incorporation resulted in even more improved photoactivity of TiO_2 leading to an optimal photoconversion efficiency of 0.63 % at the potential of 0.29 V. Remarkably low photocurrent saturation potentials of 0.29 and 0.24 V *vs.* Ag/AgCl were obtained for TNTA with and without porphyrin, respectively, confirming very efficient charge separation and transportation through the photoanode [13].

The PEC performance and solar to hydrogen efficiency can be evaluated directly by the photocurrent density which is related to the rate of interfacial electron transfer. The experiment was carried out without applying any filters in order to examine the effect of light heat on the durability of the porphyrin. No detrimental effect was observed for the TNTA and TNTA embedded with porphyrins operating even up to 4 h of irradiation. The TNTA/Cu-porphyrin electrode, however, showed an increasing photocurrent response over the test time reaching the photo current generated by the pure TNTA electrode (comparison of the three electrode samples are given in Fig. S7). This behaviour could be attributed to the agglomeration of the Cu-porphyrin on the TNTA surface which blocks the tubular structure of the TiO_2 and limited the accessibility of the ionic species. The oxygen generation and long term stability of annealed TNTA and TNTA/porphyrins have been studied and plotted in Fig. 5 (c). As it can be seen, the photocurrent of TNTA/Porphyrin reaches 1.8 mAcm^{-2}, whereas the pure TNTA only contributes 1.35 mA cm^{-2} at 1.1 V. Sustainable photocurrent generations in the process are clearly obvious for both TNTA with and without porphyrin, indicating good physical binding between porphyrin and TiO_2 nanotube arrays. Gas chromatograph (GC) was also performed over the course of amperometric tests allowing gas quantity measurement and quantifying the evolved oxygen. Initial oxygen generation rates of 328 and 155 were increased to 436 and 380 µL h^{-1} after 3 hours amperometric test, for the TNTA with and without porphyrin, respectively. The O_2 production rate is much higher than that obtained for conventional TiO_2 at neutral pH conditions [37]. Increased oxygen generation rate of the porphyrin-containing electrode is consistent with the observed catalytic activity. The obtained high rate of gas generation of the sample corresponds to high faradaic efficiency listed in Table S1 (Supporting Information). The enhanced gas production rate can be a result of the localized acidification from the water disassociation over the course of applied potential (the pH measurement of the H-cell compartments confirmed the pH degradation). Generally, the phosphonate anchoring group porphyrin offers a very stable and strong linkage to TiO_2 surface over a wide pH range [38]. The stronger binding is, therefore, responsible for retention of current density of TiO_2/porphyrin over the long term stability performance.

Conclusions

In summary, we have studied the effect of the heat treatment regime on tuning the bandgap structure of TiO_2 nanotubes prepared by anodic oxidation through controlled anatase to rutile transformation. It was found that annealing TiO_2 nanotube under an argon environment is an effective method to introduce undercoordinated Ti atoms and oxygen vacancies resulting in the formation of mid-gap electronic states and bandgap narrowing. Paying particular attention to the oxygen evolution reaction, it was found that the energy positions of localized states would contribute to the high performance oxygen generation in photo-electrochemical water splitting. Our work has demonstrated a simple and yet economic and green strategy to synthesize a fairly stable TiO_2 nanotube which can effectively decrease the overpotential for water oxidation.

Furthermore, sustainable oxygen production from water was also achieved using both pure and porphyrin containing TNTA electrodes with the photoconversion efficiency of 0.45% and 0.63% at a very low potential of 0.24 V and 0.29 *vs.* Ag/AgCl.

Acknowledgements

Financial support from the ARC Centre of Excellence for Electromaterials Science (ACES) are gratefully acknowledged. We would like to thank Prof. David L. Officer, Dr. Andrew Nattestad and Dr. Dennis Antiohos for valuable discussion. The authors also acknowledge use of the facilities at the AIIM Electron Microscopy Centre, and Australian National Fabrication Facility (ANFF).

Notes and references

[a] ARC Centre of Excellence for Electromaterials Science, Intelligent Polymer Research Institute, University of Wollongong, Wollongong, NSW, 2500, Australia.

[b] Institute for Superconducting and Electronic Materials, ARC Centre for Electromaterials Science, University of Wollongong, Wollongong, NSW, 2500, Australia.

Electronic Supplementary Information (ESI) available: [details of any supplementary information available should be included here]. See DOI: 10.1039/b000000x/

1. S. Y. Reece, J. A. Hamel, K. Sung, T. D. Jarvi, A. J. Esswein, J. J. H. Pijpers and D. G. Nocera, *Science*, 2011, **334**, 645-648.
2. T. Hisatomi, J. Kubota and K. Domen, *Chemical Society Reviews*, 2014.
3. J. H. Park, S. Kim and A. J. Bard, *Nano Letters*, 2005, **6**, 24-28.
4. A. Currao, *CHIMIA International Journal for Chemistry*, 2007, **61**, 815-819.
5. L. Duan, F. Bozoglian, S. Mandal, B. Stewart, T. Privalov, A. Llobet and L. Sun, *Nat Chem*, 2012, **4**, 418-423.
6. Q. Kang, J. Cao, Y. Zhang, L. Liu, H. Xu and J. Ye, *Journal of Materials Chemistry A*, 2013, **1**, 5766-5774.
7. W. Zhao, X. Wang, H. Sang and K. Wang, *Chinese Journal of Chemistry*, 2013, **31**, 415-420.
8. B. Liu, X. Zhao, Q. Zhao, X. He and J. Feng, *Journal of Electron Spectroscopy and Related Phenomena*, 2005, **148**, 158-163.
9. M. Kong, Y. Li, X. Chen, T. Tian, P. Fang, F. Zheng and X. Zhao, *Journal of the American Chemical Society*, 2011, **133**, 16414-16417.
10. L. Li, J. Yan, T. Wang, Z.-J. Zhao, J. Zhang, J. Gong and N. Guan, *Nat Commun*, 2015, **6**.
11. G. Liu, C. Sun, H. G. Yang, S. C. Smith, L. Wang, G. Q. Lu and H.-M. Cheng, *Chemical Communications*, 2010, **46**, 755-757.
12. X. Chen, L. Liu, P. Y. Yu and S. S. Mao, *Science*, 2011, **331**, 746-750.
13. G. Wang, H. Wang, Y. Ling, Y. Tang, X. Yang, R. C. Fitzmorris, C. Wang, J. Z. Zhang and Y. Li, *Nano Letters*, 2011, **11**, 3026-3033.
14. F. E. Osterloh and P. B. A, *MRS Bulletin*, 2011, **36**, 17-22.
15. M. Salari, S. H. Aboutalebi, A. T. Chidembo, I. P. Nevirkovets, K. Konstantinov and H. K. Liu, *Physical Chemistry Chemical Physics*, 2012, **14**, 4770-4779.
16. M. Salari, K. Konstantinov and H. K. Liu, *Journal of Materials Chemistry*, 2011, **21**, 5128-5133.
17. M. Salari, S. H. Aboutalebi, A. T. Chidembo, K. Konstantinov and H. K. Liu, *Journal of Alloys and Compounds*, 2014, **586**, 197-201.
18. P. Roy, S. Berger and P. Schmuki, *Angewandte Chemie International Edition*, 2011, **50**, 2904-2939.
19. P. P. Vijayan, M. Thomas and K. C. George, *Journal of Applied Physics*, 2012, **112**, 104308-104308.
20. J. R. Swierk and T. E. Mallouk, *Chemical Society Reviews*, 2013, **42**, 2357-2387.
21. C. C. Mercado, F. J. Knorr, J. L. McHale, S. M. Usmani, A. S. Ichimura and L. V. Saraf, *The Journal of Physical Chemistry C*, 2012, **116**, 10796-10804.
22. H. Xu, P. Reunchan, S. Ouyang, H. Tong, N. Umezawa, T. Kako and J. Ye, *Chemistry of Materials*, 2013, **25**, 405-411.
23. J. Shi, J. Chen, Z. Feng, T. Chen, Y. Lian, X. Wang and C. Li, *The Journal of Physical Chemistry C*, 2006, **111**, 693-699.
24. N. D. Abazović, M. I. Čomor, M. D. Dramićanin, D. J. Jovanović, S. P. Ahrenkiel and J. M. Nedeljković, *The Journal of Physical Chemistry B*, 2006, **110**, 25366-25370.
25. N. Daude, C. Gout and C. Jouanin, *Physical Review B*, 1977, **15**, 3229-3235.
26. L. Fleming, C. C. Fulton, G. Lucovsky, J. E. Rowe, M. D. Ulrich and J. Lüning, *Journal of Applied Physics*, 2007, **102**, -.
27. D. O. Scanlon, C. W. Dunnill, J. Buckeridge, S. A. Shevlin, A. J. Logsdail, S. M. Woodley, C. R. A. Catlow, M. J. Powell, R. G. Palgrave, I. P. Parkin, G. W. Watson, T. W. Keal, P. Sherwood, A. Walsh and A. A. Sokol, *Nat Mater*, 2013, **12**, 798-801.
28. R. van de Krol, Y. Liang and J. Schoonman, *Journal of Materials Chemistry*, 2008, **18**, 2311-2320.
29. A. Thomas, *Physical review. B, Condensed matter*, 2003, **67**, 035110.
30. W.-J. Yin, S. Chen, J.-H. Yang, X.-G. Gong, Y. Yan and S.-H. Wei, *Applied Physics Letters*, 2010, **96**, -.
31. M. Salari, S. H. Aboutalebi, K. Konstantinov and H. K. Liu, *Physical Chemistry Chemical Physics*, 2011, **13**, 5038-5041.
32. F. D. Hardcastle, *Journal of the Arkansas Academy of Science*, 2011, **65**, 43.
33. M. J. Griffith, K. Sunahara, P. Wagner, K. Wagner, G. G. Wallace, D. L. Officer, A. Furube, R. Katoh, S. Mori and A. J. Mozer, *Chemical Communications*, 2012, **48**, 4145-4162.
34. S. K. Mohapatra, M. Misra, V. K. Mahajan and K. S. Raja, *The Journal of Physical Chemistry C*, 2007, **111**, 8677-8685.
35. B. Chen, J. Hou and K. Lu, *Langmuir*, 2013, **29**, 5911-5919.
36. J. Benton, J. Bai and T. Wang, *Applied Physics Letters*, 2013, **102**, -.
37. E. Selli, G. L. Chiarello, E. Quartarone, P. Mustarelli, I. Rossetti and L. Forni, *Chemical Communications*, 2007, 5022-5024.
38. H. Park, E. Bae, J.-J. Lee, J. Park and W. Choi, *The Journal of Physical Chemistry B*, 2006, **110**, 8740-8749.